ARTICLE NO. 79-0153R

# Engineering Model for Re-entry Vehicle Turbulent Wakes

T.C. Lin,* J.B. Fedele,† R.L. Baker,* and B.M. Pershing*
*The Aerospace Corporation, Los Angeles, Calif.*

**An engineering model for the supersonic portion of the turbulent near wake behind a re-entry vehicle is presented. By treating only the supersonic regions, the saddle-point singularities present in the full formulation of the near-wake problem are avoided, and a system of equations is obtained which is solved in approximately one minute of CDC 7600 computer time using forward-marching numerics and incorporating a two-parameter mixing length model. The model is applied to decelerator performance, and the results agree favorably with wind-tunnel data. The model is also applied to near-wake electron density predictions, and the results are reasonable.**

## Introduction

THE low-altitude, near-wake flowfield properties behind a high-speed re-entry vehicle have long been of interest to the aeronautical community. The interest has been greatly stimulated by the need to monitor and predict the observable characteristics of both the near and far wake. The recent efforts and developments in re-entry vehicle decelerator concepts[1,2] have further increased the need for engineering estimates and calculations of the near-wake properties.

Past mathematical treatments of the base flow and wake properties for problems of this type can be divided into two categories: 1) Navier-Stokes model, and 2) modified boundary-layer formulation with eigenvalue parameters. Examples of the first category are the calculations of Ross and Cheng[3] and Weiss et al.[4] In the former case, a time-dependent, explicit, iterative finite-difference scheme is used for the laminar near wake. In the Weiss formulation, the laminar near wake between the base and rear stagnation point is divided into three regions. An inviscid rotational method-of-characteristics procedure is used for the expansion and recompression of the body flow at the base. Boundary-layer equations are used to describe the viscous shear layer that separates the expansion region from the recirculation region. A finite-difference solution to the steady Navier-Stokes equations is used for the recirculation region, which is iteratively matched to the shear region along the dividing streamline.

In the second category, Ohrenberger and Baum[5,6] have developed a steady-state modified boundary-layer-eigenvalue approach, and have obtained favorable comparisons with laminar experiments.[7] Their model divides the near wake into two regions that are interior and exterior to a "matching" streamline. The exterior flow is described by an implicit finite-difference method with forward marching in the streamwise direction, while an integral method is applied to the inner region (which contains the recirculation region). The presence of saddle-point singularities in both the outer flow (located in the wake neck region) and the inner flow (at the wake stagnation point) complicates the calculation procedure. Ohrenberger has recently extended the model to turbulent near wakes[7,8] by employing model equations for the turbulent kinetic energy and the dissipation rate of turbulence. For either laminar or turbulent flows, the method requires skill and experience to carry out the calculations routinely as an engineering tool.

The present work resulted from a need for a fast, easy-to-use engineering tool for the prediction of re-entry vehicle near-wake radar observables and decelerator drag, particularly at altitudes below boundary-layer transition. This paper describes such a model which contains the pertinent physics and produces reasonable results. This is accomplished by restricting the analysis to only the supersonic regions of the wake. This is sufficient for the determination of decelerator drag at distances greater than 3-5 base diameters downstream behind the base of an RV (re-entry vehicle), and for the determination of low-altitude, near-wake, low-frequency radar observables, as will be shown later. The model presented herein requires approximately one minute of CDC 7600 computer time to determine the flow properties (in the supersonic portion of the wake) out to twenty base diameters behind the body. It can thus be used routinely as an engineering tool for parametric studies. The model neglects the base recirculation region (and adjoining shear layer) and hence requires additional information (such as the base pressure) in order to obtain the recirculation region boundary. This is in contrast to the fully coupled methods previously described where the entire near-wake flow properties, including base pressure and recirculation region properties, are calculated. For the present method, a prediction of the entire near wake is not attempted in order to obtain speed and ease of use in describing the relevant supersonic wake regions.

## Formulation

Figure 1 schematically depicts the axisymmetric near-wake geometry considered. The lower boundaries of the calculation domain are the "boundary" streamline and the axis of symmetry downstream of the boundary streamline. The subsonic portion of the wake, which lies below the boundary streamline and is not considered, includes the recirculation zone and shear layer, the wake stagnation point, and the subsonic portion of the wake neck region. The calculation domain is bounded on the left by the starting data line consisting of the inviscid shock layer and the boundary-layer profiles at the end of the vehicle. The calculation involves forward streamwise marching numerics commencing from the

Presented as Paper 79-0153 at the 17th Aerospace Sciences Meeting, New Orleans, La., Jan. 15-17, 1979; submitted Feb. 16, 1979; revision received July 17, 1979. 

Index categories: Computational Methods; Jets, Wakes, and Viscid-Inviscid Flow Interactions; Supersonic and Hypersonic Flow.

*Member of the Technical Staff, Fluid Dynamics Department. Member AIAA.

†Plasma Physics Office, Fluid Dynamics Department.

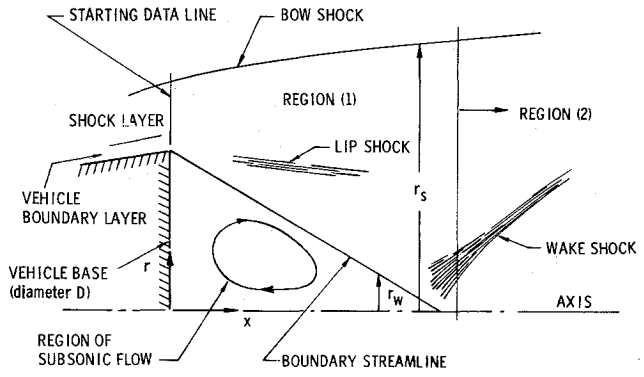


**Fig. 1 Wake flowfield schematic.**

starting data line and proceeding downstream to any desired location.

The domain of interest is divided into two regions. In the first region, the expansion (and recompression) of the frustum boundary layer and shock layer is the dominant physical process. The flow can be assumed to be inviscid since pressure gradient and convection effects are of primary importance. The flow, however, is rotational and the entropy and total enthalpy can vary from streamline to streamline. The location of the boundary streamline must be specified (by experiment or analysis) in order to solve for the first region flowfield properties. In the example calculations performed later, the boundary streamline is taken to be at a slope determined by isentropically expanding a near-wall supersonic point in the boundary layer to the vehicle base pressure. The base pressure is an input parameter that is obtained from experimental data, empirical correlations, and so forth. In the present work, for turbulent flows, the Cassanto et al.[9] correlation of base pressure with boundary layer pressure and edge Mach number was used to obtain the base pressure. Expansion of the $M=2$ point in the boundary layer, to the base pressure, resulted in supersonic flow everywhere, including the compression through the wake shock.

The second region begins just beyond the point where the boundary streamline intersects the axis. In this region, the pressure gradient is not dominant (except across the wake shock), and it is necessary to include turbulent transport in the model. The governing equations for these two regions are:

Continuity

$$\frac{\partial}{\partial x}(\rho u)+\frac{\partial}{\partial r}(\rho v)+\frac{\rho v}{r}=0 \tag{1}$$

$x$-Momentum

$$\frac{\partial}{\partial x}(p+\rho u^2)+\frac{\partial}{\partial r}(\rho uv)+\frac{\rho uv}{r}=\frac{\epsilon\partial}{r\partial r}\left[(\mu+\mu_t)r\frac{\partial u}{\partial r}\right] \tag{2}$$

$r$-Momentum

$$\frac{\partial}{\partial x}(\rho uv)+\frac{\partial}{\partial r}(p+\rho v^2)+\frac{\rho v^2}{r}$$
$$=\epsilon\frac{\partial}{\partial r}\left\{(\mu+\mu_t)\left[2\frac{\partial v}{\partial r}-\frac{2}{3}\left(\frac{\partial v}{\partial r}+\frac{v}{r}+\frac{\partial u}{\partial x}\right)\right]\right\}$$
$$+2\epsilon\frac{(\mu+\mu_t)}{r}\left(\frac{\partial v}{\partial r}-\frac{v}{r}\right)+\epsilon\frac{\partial}{\partial x}\left[(\mu+\mu_t)\frac{\partial u}{\partial r}\right] \tag{3}$$

Energy

$$\rho uc_v\frac{\partial T}{\partial x}+\rho vc_v\frac{\partial T}{\partial r}+p\left[\frac{\partial u}{\partial x}+\frac{\partial v}{\partial r}+\frac{v}{r}\right]$$
$$=(\mu+\mu_t)\epsilon\left(\frac{\partial u}{\partial r}\right)^2+\frac{\epsilon}{r}\frac{\partial}{\partial r}\left[(K+K_t)r\frac{\partial T}{\partial r}\right] \tag{4}$$

State

$$p=p(\rho,T) \tag{5}$$

where $\epsilon=0$ in region 1 and $\epsilon=1$ in region 2.

Prandtl's modified (two-parameter) mixing length model is used to specify the eddy viscosity

$$\mu_t=\rho l_1^2\left[\left(\frac{\partial u}{\partial r}\right)^2+l_2^2\left(\frac{\partial^2 u}{\partial r^2}\right)^2\right]^{1/2} \tag{6}$$

Rudy and Bushnell[10] related the mixing length parameters $l_1$ and $l_2$ to the characteristic wake width in the following manner:

$$l_1=l_2=0.05\delta \tag{7}$$

with $\delta=1.2r_{0.95}+x\tan(8\text{ deg})$ for $\delta<2.4r_{0.95}$ and $\delta=2.4r_{0.95}$; otherwise, where $r_{0.95}$ is the location where

$$(u-u_\xi)/(u_e-u_\xi)=0.95$$

They found that this formulation produced results which agreed well with the axisymmetric wake data of Chevray.[11] The turbulent heat conductivity $K_t$ is related to $\mu_t$ by taking a value of 0.9, for instance, for the turbulent Prandtl number. For laminar flow calculations, $\mu_t$ and $K_t$ are set equal to zero.

Equations (1-7) form a closed set of equations for the flow variables $p$, $\rho$, $T$, $u$, and $v$. A coordinate transformation from $r$, $x$ to $\eta=(r-r_w)/(r_s-r_w)$, $x/D$ is employed in region 1 and $r$, $x$ to $\xi=r/x$, $x/D$ in region 2. The equations are integrated using MacCormack's[12,13] two-level explicit scheme, commencing at the starting data line using shock-layer and boundary-layer profiles, and marching downstream. (There are many methods and computer codes for obtaining the shock-layer and boundary-layer fluid mechanical properties.) The bow shock is treated as a discontinuity across which the Rankine-Hugoniot conditions apply. Its shape is calculated step by step as part of the calculation procedure.[13] The imbedded lip shock and wake shock are treated by the shock-capturing technique. The inviscid equations are integrated to the region 1-region 2 interface, and the solution at the interface is used for the starting line conditions for the integration of the viscid equations. The marching step size in region 1 is limited by the Courant-Frederick-Levy condition. In the viscous region 2, this condition was often found to be overly restrictive; it can be relaxed if a further decrease in machine running time is desired.

The solution procedure is completed by appropriate boundary conditions at the lower boundaries. Along the boundary streamline (see Fig. 1) the entropy and total enthalpy are constant, and the velocity component normal to the boundary vanishes. The pressure along the boundary streamline is obtained from the compatibility relation along right running characteristics terminating at the boundary.[13] The wake centerline is an axis of symmetry. Along the axis downstream of the boundary streamline, symmetry conditions of $v=0$, $\partial/\partial r=0$ apply. Convenient fluid mechanical variables to be specified along the starting line are $p$, $u$, $v$, and $T$.

In region 1, a large flow expansion occurs from the vehicle surface to the boundary streamline, and the calculation for the interior points downstream of the expansion may become ill-behaved. Numerical oscillations could appear in the flow variables which can eventually produce negative pressure at isolated points in the interior flowfields. When such a situation occurs, the numerical marching step size is reduced, and, if needed, a heuristic smoothing scheme suggested by Solomon et al.[14] is employed. When the local pressure in either the predictor or corrector of MacCormack's scheme is negative at an interior point, then the local conservation vector is redefined as

$$\tilde{E}_{I,J}=[E_{I+1,J}+E_{I,J}+E_{I-1,J}]/3$$

where vector

$$E=\begin{bmatrix}\rho u\\ \rho u^2+p\\ \rho uv\\ \rho eu\end{bmatrix} \quad \text{[see Eqs. (1-4)]}$$

The application of this type of local smoothing can be shown to yield a first-order accurate approximation for smooth flow problems. There is no such difficulty in region 2.

The method described herein provides for the complete calculation of the supersonic wake flow. The model results in a well-posed initial-line explicit forward-marching scheme with no mathematical singularities. The accuracy of the method depends on the insensitivity of the outer inviscid flow to changes in the recirculatory region. For instance, Ross and Cheng[3] have shown that the expansion-dominated outer-inviscid region is much more sensitive to changes in the vehicle boundary-layer and shock-layer properties than to changes in the recirculatory wake geometry. Thus, a reasonable method of determining the slope of the "boundary" streamline in region 1 should suffice. Further downstream in region 2, the effect of the neglect of the shear and recirculatory flow should be primarily confined to the near-axis flow. The total drag on a downstream drogue does not depend critically on the near-axis flow which intercepts only a small portion of the drogue frontal area. For most wake radar observables applications, the near-wake electron densities in the outer flow away from the boundary streamline in region 1 and away from the axis in region 2 are sufficiently high so that little electromagnetic energy can propagate into the shear layer or recirculation region, or into the near-axis region downstream.

The eddy viscosity model used is consistent with the development of an engineering tool. The drogue drag calculation depends on a radial integration of a weighted dynamic pressure [see Eq. (8)] and, therefore, is not sensitive to the details of the near-axis flow which is dominated by small-scale turbulence. The radar application also is not sensitive to the details of the near-centerline flow. The details of a specific turbulence model are expected to be more important near the axis than in the outer flow. The engineering turbulence model used here contains sufficient information for the application herein, but may not be appropriate for applications where the details of the small-scale turbulence are important.

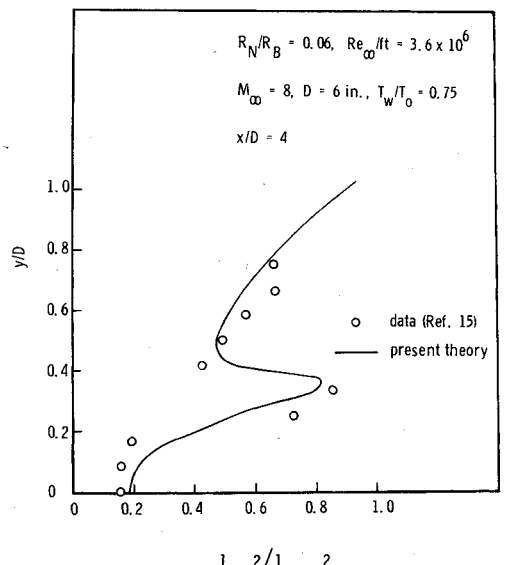


**Fig. 2 Dynamic pressure profile at $x/D=4$.**

Wake flowfield profiles calculated by the model were compared with available wind-tunnel data[15] and were found to agree reasonably well. A comparison of the measured pitot pressure profile with that predicted by the model at four base diameters downstream from the base of a sphere-cone body is shown in Fig. 2.

## Applications

### Mass-Jettison Drag Prediction

One method of initiating the soft recovery of an RV is by ejection of part of its mass into the wake. A knowledge of the drag of the ejected mass is necessary for the prediction of separation dynamics and the design of the ejection system. Two types of wake flow, open or closed wake, have been observed to occur for the flow around a forebody or afterbody. These flow geometries are illustrated in Fig. 3. In an open wake flow, the region between the forebody (the RV) and the afterbody is completely separated as the freestream flow jumps across the gap. For this case, the pressure recovery, and hence the drag, on the afterbody is small, endangering the separation between the forebody and afterbody. The closed wake structure shows the typical wake formation behind the forebody and a flow about the afterbody which is dependent upon the afterbody geometry. Charwat et al.[16] found that a critical distance between a fore and aft body exists, such that the wake is open for separation distances less than this critical distance and closed at greater distance. Charwat's wind-tunnel data indicated that for aft to forebody diameter ratios of the order of one, the critical distance is between two and three forebody base diameters aft of the forebody base.

Thomas et al.[17] in the turbulent, high-speed wake experiments found that the drag on the afterbody when it was between approximately two and three forebody diameters behind the forebody was not a unique function of position, but was dependent upon the direction (upstream or downstream) from which the afterbody reached that position. The difference in drag depended on whether the wake was open or closed. The critical distance for a closed wake was found to be less if the afterbody is brought in from downstream rather than from upstream. However, the change in critical distance was not large. The data also indicate that the critical distance

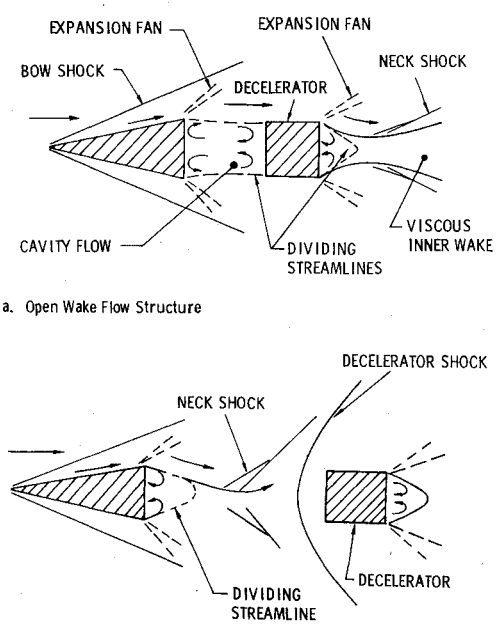


**Fig. 3 Two possible flow geometries about a vehicle/decelerator configuration.**

for high-speed turbulent wakes is almost independent of Mach number and that laminar wakes are more sensitive to disturbances than turbulent wakes and are expected to have larger critical distances than turbulent wakes.

The present wake model computes the free wake and is not applicable to open-wake configurations. In general, separation systems are designed to propel the mass-jettison body beyond the critical distance needed for a closed turbulent wake. Therefore, analysis of an open wake is not needed to assess the performance of a mass-jettison system. In the case considered below, drogue drag calculations are compared to AEDC data.[18] The wakes in the AEDC experiments were turbulent and closed.

The surface pressure on the decelerator (mass-jettison afterbody) located in the wake flow can be estimated by time-dependent blunt-body calculations. One example of this type of computation was carried out in Ref. 19. However, Crowell[20] has shown that in certain cases a modified Newtonian theory, which properly takes into account the freestream nonuniform flow, can predict the blunt-body surface pressure reasonably well. Using such an approach, the following relation is employed to calculate the jettison drag

$$C_D = \frac{C_{p_s}}{A}\int_0^r 2\pi r \frac{q}{q_\infty}\sin^2(\theta_d - \theta_f)\,dr$$

$$= \text{decelerator drag in closed wake flow} \qquad (8)$$

where

$\theta_d, \theta_f$ = local body slope and flow inclination, respectively
$C_{p_s}$ = 1.6 (for flat face cylinder)
$q_\infty$ = freestream dynamic pressure in front of the RV
$q$ = local undisturbed dynamic pressure in front of the decelerator

where $q$ is obtained from the wake flow model described earlier. Equation (8) is based on a modified Newtonian theory corrected to account for variation in dynamic pressure in the wake. This equation asymptotes to the flat face cylinder drag when the flat-faced decelerator is placed in a uniform freestream.

Drag calculations were performed for the blunt jettison-decelerator shown in Fig. 4. Figure 5 gives the predicted and measured jettison drag coefficient as a function of freestream Mach number at $x/D = 3$. The general trend is that the $C_D$ becomes smaller as $M_\infty$ increases. This type of variation is expected, since the total pressure loss across a shock becomes larger as the Mach number increases. As shown in Fig. 5, the present numerical results agree favorably with the AEDC-VKF-Tunnel F measurements.

Calculations were also performed for the drag on the decelerator as a function of decelerator location downstream from the RV main body and are shown in Fig. 6. This figure illustrates the increasing importance of turbulent mixing as the flow progresses downstream. The present model, without considering the turbulent mixing process, predicts that the $C_D$ decreases slightly with $x$ for $x/D > 3$. However, when turbulent transport is included in the model, the predicted trend agrees with the experimental trend (see Fig. 6). The turbulent wake width at $x/D$ values of interest is much larger than the afterbody (see Fig. 2). The turbulent mixing decreases the wake velocity defect and, therefore, increases the dynamic pressure experienced by the afterbody, resulting in greater drag relative to the no-mixing case.

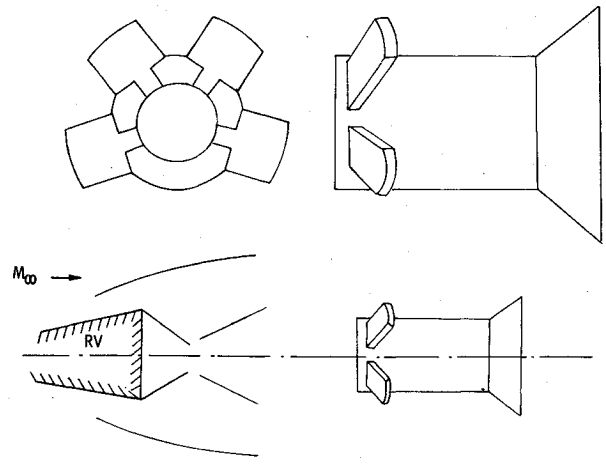


Fig. 4 Mass-jettison configuration.

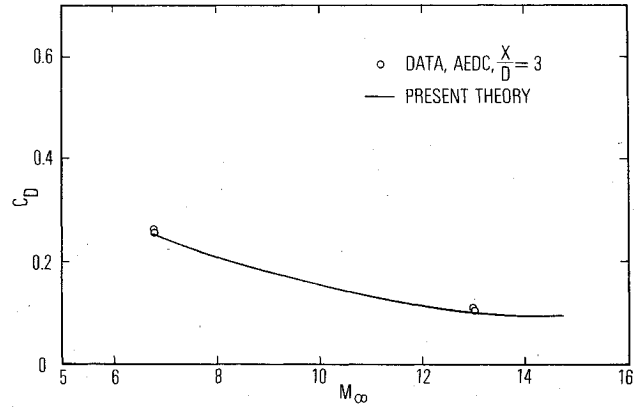


Fig. 5 Mass-jettison drag vs freestream Mach number.

### Wake Electron Density Predictions

The model's second application involves the prediction of turbulent near-wake electron density profiles. Near-wake electron densities are needed for the determination of radar observables. For the prediction of electron density, the boundary-layer and shock-layer starting line data must include the electron mass fraction, and the electron species continuity equation must be added to the set of equations to be solved in the wake.

The low-altitude electron flux into the turbulent near wake of a re-entry vehicle is dominated by the ionization of alkali contaminants (primarily sodium) in the vehicle heat shield. Even for moderately blunt vehicles, the low-altitude clean air ionization contribution is usually small compared to the sodium contribution. For examples given here, the dominant positive ion will be assumed to be $Na^+$. In the expansion-dominated region 1, the electron chemistry may be taken to be frozen. In the viscous region 2, the turbulent diffusion of electrons is very important. Also, in order to obtain accurate estimates of electron density beyond five base diameters or so downstream of the base, the electron recombination chemistry must be considered. For the low-altitude supersonic near wake, electron generation is not important. The temperature is not high enough to produce significant clean air ionization, and the sodium heat shield contaminants are already nearly all ionized within the hot vehicle boundary layer. The electron chemical decay begins primarily by three-body sodium ion-electron recombination with a neutral particle as the third collison partner

$$Na^+ + e^- + M \rightarrow Na + M$$

The electron recombination then varies as the product of neutral density (which is approximately the overall density) and the square of the electron density. Using the sodium ion recombination rate of Jensen and Padley[21] which has a $1/T^2$ temperature dependence, the electron species equation for the

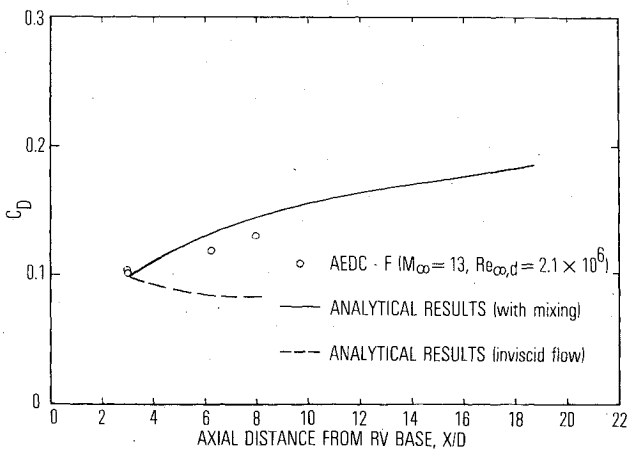


**Fig. 6 Mass-jettison drag vs $x/D$.**

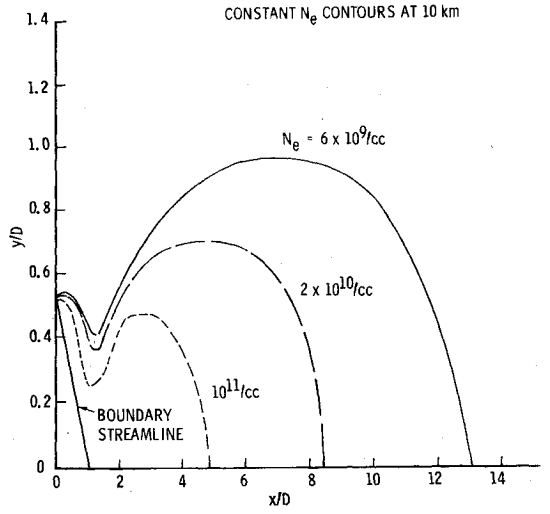


**Fig. 7 Electron density contour in the wake.**

electron mass fraction $C$ becomes

$$\rho u\frac{\partial C}{\partial x}+\rho v\frac{\partial C}{\partial r}=\epsilon\left\{\frac{1}{r}\frac{\partial}{\partial r}\left[\rho(D+D_t)r\frac{\partial C}{\partial r}\right]-K_r\rho^3C^2/T^2\right\} \quad (9)$$

where, as before, $\epsilon=0$ in region 1 and $\epsilon=1$ in region 2.

The fluid mechanical variables are not affected by the presence of the trace constituents, so that Eq. (9) is decoupled from the rest of the flowfield equations. Once $\rho$, $u$, $v$, $p$, and $T$ are obtained using Eqs. (1-7), then $C$ can be obtained using Eq. (9). The turbulent diffusivity $D_t$ was obtained from $\mu_T$ by taking a turbulent Schmidt number of unity. The molecular Schmidt number was also taken as unity, and the molecular and turbulent Prandtl numbers were taken as 0.72 and 0.9, respectively, in the calculations. Along the boundary streamline, which is contained within region 1, $C$ is constant. Along the axis ($r=0$) downstream of the boundary streamline, the boundary condition $\partial C/\partial r=0$ is applicable.

Typical low-altitude (10 km) near-wake electron density contours for a slender conical RV are shown in Fig. 7. As the boundary layer expands off the base into region 1, where the electron mass fraction is constant along streamlines, the electron density decreases as the mass density decreases. As the flow begins to turn parallel to the axis and crosses the wake shock, the electron density increases as the mass density increases. As the flow progresses further downstream into region 2, electron recombination reduces the electron density, and the turbulent diffusion decreases the radial electron density gradient and broadens the profile. As shown in Fig. 7, the $10^{11}$/cc contour becomes very flat just beyond $x/D=4$, the $2\times10^{10}$ contour just beyond $x/D=8$, and so forth. The effect of including electron recombination was to reduce the electron density by a factor of two to three at $x/D=12$ (compared to a calculation for $K_r\equiv0$).

The location of the boundary streamline, as shown in Fig. 7, is below the location of the $10^{11}$/cc electron density contour. The inviscidly determined electron densities at the dividing boundary streamline are greater than $10^{12}$ electrons/cc. The critical electron density for which the plasma is overdense at S-band (~2.5 GHz) is $8\times10^{10}$. Thus, electromagnetic energy at a frequency of at least as large as S-band would not be expected to propagate into the high electron density region near the boundary streamline. It was previously mentioned that the outer inviscid region is not greatly affected by geometry changes in the recirculation region. Thus, with the outer region largely unaffected by the location of the boundary streamline and the electromagnetic energy at most radar frequencies of interest not propagating into the near vicinity of the streamline, the precise determination of the location for a "boundary" for the supersonic inviscid region is not critical.

The total accuracy of near-wake electron density predictions cannot be definitively assessed. There are no direct measurements of near-wake electron densities. There are some radar cross section data on the near wake, but determination of plasma properties from the data involves large uncertainties. The electron density profile shapes predicted do appear to be reasonable with regard to the physics of the problem.

## Summary

An engineering model for the supersonic portion of the axisymmetric near-wake flow is presented. For turbulent flow, a two-parameter modified Prandtl mixing length model is used for the eddy viscosity. A boundary streamline, whose slope must be specified apart from the method, separates the inviscid supersonic expansion-dominated region just beyond the end of the frustum from the recirculatory region. In the examples presented herein, this slope is determined by isentropic expansion of the boundary layer to the base pressure, which can be determined from correlations appearing in the literature. Downstream of the intersection of the boundary streamline and the wake axis, molecular and turbulent transport are considered.

The model was applied to the calculation of the drag of a near-wake mass-jettison vehicle decelerator and to the calculation of near-wake electron densities. Comparison of calculations with near-wake wind tunnel pitot pressure profiles was favorable, as was the comparison of the predicted decelerator drag with wind tunnel decelerator drag data. The predicted electron density profiles appear reasonable, but lack of data prevents definitive substantiation of their accuracy. For these applications, approximately one minute of CDC 7600 computer time per case was required.

## References

[1] Atkinson, C.A. and Haigh, W.W., "Decelerator Performance Study—Final Report," SAMSO-TR-70-48, March 1970.

[2] English, E.A., "Nosetip Recovery Vehicle Postflight Development Report," SAND 75-8059, Jan. 1976 (unlimited release).

[3] Ross, B.B. and Cheng, S.I., "The Application of Finite Difference Methods to the Supersonic Near Wake," AIAA Paper 72-115, AIAA 10th Aerospace Sciences Meeting, San Diego, Calif., Jan. 1972.

[4] Weiss, R.F., Greenberg, R.A., and Biondo, P.P., "A New Theoretical Solution of the Laminar, Hypersonic Near Wake," Avco Research Rept. 256, Aug. 1966.

[5] Ohrenberger, J.T. and Baum, E., "A Theoretical Model of the Near Wake of a Slender Body in Supersonic Flow," *AIAA Journal*, Vol. 10, Sept. 1972, pp. 1165-1172.

[6]Ohrenberger, J.T. and Baum, E., "Laminar Near Wake Solution under Atmospheric Entry Conditions," AIAA Paper 72-116, AIAA 10th Aerospace Sciences Meeting, San Diego, Calif., Jan. 1972.

[7]Ohrenberger, J.T. and Baum, E., "Theoretical Modeling of the Base Flow Region of Supersonic Bodies: A Steady-State Method," *Aerodynamics of Base Combustion—Progress in Astronautics and Aeronautics,* Vol. 40, edited by Murthy, The MIT Press, 1976.

[8]Ohrenberger, J.T., "Flow Properties in the Near Wake of Hypersonic Vehicles at Low Altitudes," Hanscom AFB-RADC/ETEP Rept. RADCTR-76-298, Sept. 1976.

[9]Cassanto, J.M., Rasmussen, N.S., and Coats, J.D., "Correlation of Free-Flight Base Pressure Data for M=4 to 19," *AIAA Journal,* Vol. 7, June 1969, pp. 1154-1157.

[10]Rudy, D.H. and Bushnell, D.M., "A Rational Approach to the Use of Prandtl's Mixing Length Model in Free Turbulent Shear Flow Calculations," *Free Turbulent Shear Flows,* Vol. 1, NASA SP-321, 1972.

[11]Chevray, R., "The Turbulent Wake of a Body of Revolution," *Transactions of ASME, Series D: Journal of Basic Engineering,* Vol. 90, No. 2, June 1968, pp. 275-284.

[12]MacCormack, R.W., "An Introduction to Numerical Solution of the Navier-Stokes Equations," AIAA Paper 75-1, AIAA 13th Aerospace Sciences Meeting, Pasadena, Calif., Jan. 1975.

[13]Lin, T.C. and Rubin, S.G., "A Two-Layer Model for Coupled Three-Dimensional Viscous and Inviscid Flow Calculations," AIAA Paper 75-853, AIAA 8th Fluid and Plasma Dynamics Conference, Hartford, Conn., June 1975.

[14]Solomon, J.A., et al., "Three-Dimensional Supersonic Inviscid Flow Field Calculations on Reentry Vehicles with Control Surface," AIAA Paper 77-84, AIAA 15th Aerospace Sciences Meeting, Los Angeles, Calif., Jan. 1977.

[15]Martellucci, A., Trucco, H., and Agnone, A., "Measurements of the Turbulent Near Wake of a Cone at Mach 6," *AIAA Journal,* Vol. 4, March 1966; see also BSD-TR-67-229, Vol. I, Nov. 1967.

[16]Charwat, A.F., et al., "An Investigation of Separated Flows—Part I: The Pressure Field," *Journal of Aeronautical Sciences,* Vol. 28, June 1961, pp. 457-470.

[17]Thomas, K.M., et al., "Some Shock/Wind Tunnel Observations of Interference Effects in Hypersonic Wakes," AIAA Paper 69-349, AIAA 4th Aerodynamic Testing Conference, Cincinnati, Ohio, April 1969.

[18]Beale, D., "Test Results for the SAMSO/Sandia IRS Phase III Test Conducted in AEDC-VKF Tunnel F," AEDC-DR-78-22, 1978.

[19]Lin, T.C., Reeves, B.L., and Siegelman, D., "Blunt Body Problem in Nonuniform Flow Fields," *AIAA Journal,* Vol. 15, Aug. 1977, pp. 1130-1137.

[20]Crowell, P.G., "The Blunt Body Problem in an Expanding Nonuniform Flow Field," Report No. TR-0059 (S6816-76)-2, The Aerospace Corporation, El Segundo, Calif., July 1970.

[21]Jensen, D.E. and Padley, P.J., "Kinetic Studies of Ionization and Recombination Processes of Metallic Additives to Flames," 11th Symposium on Combustion (International), Berkeley, Calif., 1966, p. 351.